

Numerical analysis of a direct contact membrane distillation system using diesel internal combustion engine waste heat

Elnaz Norouzi, Chanwoo Park*

Department of Mechanical and Aerospace Engineering, University of Missouri, Columbia, MO 65211, USA, Tel. +1-573-882-6087, email: elnaz.norouzi@mail.missouri.edu (E. Norouzi), parkchanw@missouri.edu (C. Park)

Received 3 October 2017; Accepted 4 February 2018

ABSTRACT

Membrane distillation (MD) is a water treatment technology which can produce high-quality distillate using low-grade heat from waste heat sources. MD is especially promising for off-grid locations, such as disaster-stricken areas and military bases where power infrastructure is damaged or non-existent and therefore portable power generators are temporarily deployed. In this study, Direct Contact Membrane Distillation (DCMD) systems running on the waste heat from a diesel generator was numerically analyzed by using a one-dimensional thermal-hydraulic network model considering the water vapor transport across the flat-sheet membrane of the DCMD systems. The DCMD systems analysis employs two designs of the DCMD system with single and multiple membrane modules connected in a parallel arrangement. A numerical analysis considering various operating variables (concentration of sodium chloride (NaCl), flow rates, and inlet temperatures of feed and permeate streams) and a design variable (membrane module length) of the DCMD systems was performed to investigate their effects on water distillation performance and thermal efficiency. It was found from the numerical analysis that shorter membranes produce larger water mass flux at higher thermal efficiency. Furthermore, higher flow rates of the feed and permeate streams and greater Inlet Temperature Differences (ITD) between the feed and permeate streams and less NaCl concentration produce more distilled water.

Keywords: Direct contact membrane distillation; Water treatment; Waste heat; Diesel generator

1. Introduction

During the last century, water usage has increased at twice the rate of population growth. The problem is further aggravated by the lack of availability of energy needed to produce potable water. Although two-thirds of the earth's surface is covered in water, most of it is undrinkable and current desalination technologies are very energy-intensive. Therefore, a great deal of research effort has been invested in developing more efficient water desalination technologies. Comparably, membrane distillation shows great promise due to its low electricity consumption, operational pressure and temperature, and cost compared to conventional technologies such as reverse osmosis (RO) and thermal distillation [1,2]. Membrane distillation (MD) is a

water purification technology using liquid/vapor phase changes (evaporation and condensation) in which only water vapor molecules are transported through a nano-porous hydrophobic membrane driven by the vapor pressure difference created between hot (feed) and cold (permeate) fluid streams. The MD represents one of the most recent developments in thermal distillation processes despite the fact that the technology has been around since the late 60's [3]. Recently, interest in MD has been aroused by environmental and energy concerns and rising energy prices has made MD cost-competitive with conventional distillation technologies.

The current water desalination technologies in use are reverse osmosis (RO) and thermal distillation, despite the fact that these technologies are considered to be energy-intensive. Reverse osmosis is a semi-permeable mem-

*Corresponding author.

brane-based pressure-driven process, which requires very high levels of fluid pressure to allow water molecules to diffuse through the membrane and therefore suffers from a large pumping power penalty. Thermal distillation requires a fluid to be heated up to its boiling temperature and thus consumes a large amount of energy which can be seen as a disadvantage. Considering the competitors' drawbacks, the membrane distillation is a viable alternative to conventional distillation processes. Despite its low energy efficiency, MD can run on low-grade heat from waste heat sources at no extra cost. In addition to benefiting from its ability to use waste heat sources, MD also produces superior water quality compared to that of RO (100% theoretical rejection of ions for the MD) and thermal distillation (no entrainment of non-volatile species for the MD).

Four different membrane distillation configurations have been studied which mainly differ by the arrangement of their permeate channel or the manner in which this channel is operated [4–8]. In direct contact membrane distillation (DCMD) as the simplest MD configuration, the feed and permeate streams are in direct contact with the hot and cold sides of the membrane, despite the main drawback of this design being the heat lost by conduction through the membrane. In air gap membrane distillation (AGMD), the feed water is in direct contact with only the hot side of the membrane. Stagnant air is introduced between the permeate side of the membrane and the condensation surface for the permeate vapor. The benefit of this design is the reduced heat loss by conduction, but an additional resistance of mass transfer is added, which is considered to be a disadvantage. In sweeping gas membrane distillation (SGMD), non-condensable gas such as air is used to sweep the vapor on the permeate membrane side to condense outside the membrane module. The gas flow, like in AGMD, reduces the conduction heat loss across the membrane and enhances the mass diffusion of water vapor. The main disadvantage of this configuration is that a small volume of permeate diffuses in a large sweep gas volume, requiring a large condenser because of a low partial pressure in water vapor. In the vacuum membrane distillation (VMD) configuration, a vacuum pump is used to create a vacuum on the permeate membrane side. Condensation takes place outside the membrane module [7,8]. DCMD remains a good choice because of its lower mass resistance and simple design, save for its disadvantage of a higher heat conduction loss.

Membrane distillation powered by renewable and waste heat sources have shown great promise through the work of the following researchers [9–14]. Recently, Saffarini et al. carried out an economic evaluation of solar-powered DCMD systems. They reported that a DCMD system coupled with a heat recovery heat exchanger would be the most cost-effective configuration, despite the typical high conduction losses from the feed to the permeate [10]. Suarez et al. determined the experimentally fresh water production rates and the energy requirements of the components of a DCMD system coupled with a salinity gradient solar pond (SGSP) system. Their reported laboratory results showed that a DCMD/SGSP system treated approximately six times the water flow than that of a similar system consisting of an AGMD unit driven by an SGSP [11]. Sarbatly and Chiam evaluated the coupling of geothermal energy with

the VMD. They concluded that geothermal energy could reduce the total energy consumption by approximately 95% and the cost by at least \$0.72/m³ [12]. Vega-Beltran et al. evaluated the efficiency and cost of solar multi-stage MD for stand-alone seawater desalination [13].

Military forward operating bases (FOBs) and disaster stricken areas typically rely on bottled water which is needed to be constantly resupplied from unaffected areas. The cost of supplying water for these locations rivals and often exceeds the cost of supplying other valuable commodities such as fuel. In fact, for the 2005 fiscal year, the U.S. Army estimated to have spent over \$190 million dollars supplying bottled water for operations in Afghanistan. Some estimates have pegged the cost of delivering water to the front lines to be as high as \$ 50 per gallon [15]. The costliest aspect of delivering water is the loss of life of military transportation and force protection personnel.

Although MD powered by solar and geothermal energy has proven to be feasible and cost-competitive, deployment of these systems is limited to areas that have abundant solar or geothermal energy. Solar energy is available during the day and cannot reliably support the critical needs of military and disaster relief operations due to its intermittent nature. While portable and quickly deployable, solar energy requires large surface areas to be able to provide the energy required for MD, which is unfeasible for FOBs.

Critical off-grid locations often use diesel power generators as a means of producing portable and reliable electricity. Diesel generators are compact, quickly deployable, and energy-efficient, and generate immense amounts of waste heat. Harvesting the waste heat from the diesel generators can provide a reliable and consistent source of heat. In fact, over 50% of the energy from diesel fuel is wasted in the form of low and high-grade heat by the engine cooling system and exhaust, respectively. Therefore, the combined demand for potable water and electrical power in disaster stricken areas make sense to employ the MD system running on the waste heat of diesel generator.

Here, a numerical analysis using a thermal-hydraulic network model was performed for the DCMD systems running on the waste heat of the diesel engine cooling system to investigate the effects of various operating and design variables of the DCMD systems on water distillation performance and thermal efficiency.

2. Governing equations for numerical analysis of DCMD system

The schematic of the DCMD system considered for this study is depicted in Fig. 1(a). The DCMD system consists of a feed loop and a permeate loop connected by a nanoscale porous, hydrophobic membrane. Saline water was considered as feed water for the DCMD system. Each loop consists of a heat exchanger and an external connection: a heat exchanger (HX1) and brine influx (\dot{m}_b) in the feed loop, and a heat exchanger (HX2) and distillate output (\dot{m}_d) in the permeate loop. The brine influx and distillate output are at an equal flow rate for the mass balance of the DCMD system. The heat exchanger (HX1) receives the heat (Q_{in}) from the diesel engine coolant (heat source) for the feed loop, while the heat exchanger (HX2) dissipates

the same amount of heat (q_{out}) to ambient (heat sink) for the permeate loop. Therefore, it satisfies the energy balance of the DCMD system.

For the DCMD membrane in Fig. 1a, phase change occurs in the hydrophobic pores of the membrane surfaces in direct contact with the feed and permeate streams at its respective vapor pressure: evaporation (q_{fg}) on the feed side of the membrane and condensation (q_{fg}) on the permeate side. The difference between the vapor pressures set by the respective concentration of the feed stream and saturation temperatures of the feed and permeate streams is the driving force of the water vapor flow through the membrane. A parasitic conduction heat transfer, q_k (heat loss) across the solid phase of the membrane is unavoidable with any temperature difference between the fluid streams. The sensible heat carried by the feed and permeate streams flowing into the membrane is used for the latent heat required for the phase change for water distillation as well as the conduction loss. Fig. 1b shows the schematic of a DCMD system consisting of N_m membrane modules of the same length connected in parallel which was used in analysis with the results presented in Fig. 11. The main flows of the feed and permeate streams are equally divided into each membrane module flowing in a counterflow configuration.

The following assumptions were used in the numerical analysis of the DCMD system using a thermal-hydraulic network model.

- (i) There are no polarization effects for velocities, temperatures and concentrations of feed and permeate streams in the membrane channels which is filled with a mesh spacer. That is, the lateral variations of velocity, temperature and concentration are negligible and vary along only x -direction (flow directions). Therefore, the local fluid velocity, temperature and concentration on the membrane equals the bulk fluid velocity, temperature and concentration in the membrane channels, respectively. But the water vapor flow through the membrane perpendicular to the fluid flow direction in

the membrane channels is counted in this one-dimensional analysis.

The one-dimensional approach is justifiable by the fact that a mesh spacer installed in the feed and permeate channels to physically support the fragile membrane, creates strong “turbulent mixing” as the fluid flows through tortuous paths in the mesh-filled channels and therefore greatly enhances the heat and mass transfer in the channels. Phattaranawik [16] reported an experimental measurement result of the temperature polarization coefficient of spacer-filled channels to be in the range of 0.9–0.97 which means the channel flow are well mixed in a lateral direction (along the channel height), and thus, the temperature gradient in the channels are negligible in the lateral direction. Furthermore, several researchers [17,18] reported the concentration polarization coefficient (the ratio of the wall concentration to the bulk concentration) is in the range of 1.04–1.1 which suggests a negligible concentration polarization effect. Such an analogy between momentum, heat and mass transfer are well established by a boundary layer theory [19].

- (ii) Liquid flow-through across the membrane does not occur due to a high capillary pressure head in the nanopores in the hydrophobic membrane made of PTFE.
- (iii) A complete rejection of salt takes place in the DCMD and thus no trace of salt is found in the permeate water.

A one-dimensional formulation was used for the numerical analysis based on the aforementioned assumptions. The governing equations for mass, energy and concentration conservations can be expressed as a function of only the x variable which is aligned with the feed flow direction but opposite the permeate flow. The mass conservation equations of the feed and permeate streams in an infinitesimal control volume [dotted boxes in Fig. 1(a)] are given by

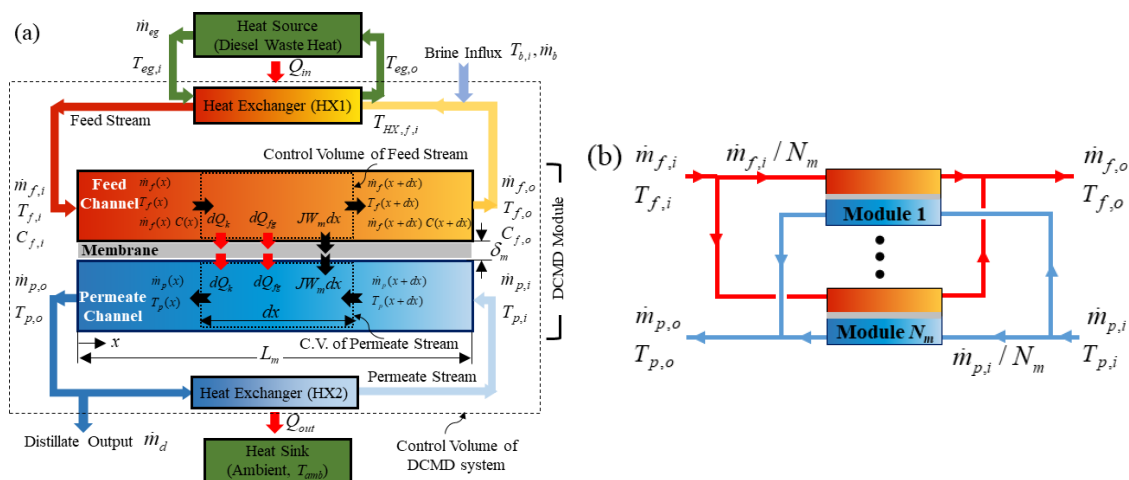


Fig. 1 (a). Schematic of a single-module DCMD system used for a thermal-hydraulic network modeling. (b) Schematic of a multiple-module DCMD system connected in a parallel arrangement.

$$\frac{\partial \dot{m}_f}{\partial x} = -JW_m, \quad (1)$$

$$\frac{\partial \dot{m}_p}{\partial x} = -JW_m, \quad (2)$$

where W_m is the widths of the membrane channels set to 1 m for simplicity. The height of the channels is not required to model the one-dimensional flow network.

The energy conservation equations for the feed and permeate streams in the membrane channels are given by

$$\dot{m}_f c_w \frac{\partial T_f}{\partial x} = c_w JW_m T_f - JW_m h_{fg} - k_m W_m \frac{T_f - T_p}{\delta_m}, \quad (3)$$

$$\dot{m}_p c_w \frac{\partial T_p}{\partial x} = c_w JW_m T_p - JW_m h_{fg} - k_m W_m \frac{T_f - T_p}{\delta_m}, \quad (4)$$

where J is the water mass flux, h_{fg} is the latent heat of evaporation or condensation, and δ_m is the thickness of the membrane. k_m is the effective thermal conductivity of the membrane and calculated by

$$k_{m,e} = (1 - \varepsilon_m)k_m + \varepsilon_m k_g, \quad (5)$$

where ε_m , k_m , and k_g are the porosity and bulk thermal conductivity of the membrane material, and thermal conductivity of water vapor, respectively.

The salt concentration in the feed channel is assumed to vary along only the flow (x) direction because of a negligible concentration polarization effect due to a strong flow mixing by a mesh spacer and can be determined based on a one-dimensional salt conservation equation and is given by

$$\frac{\partial C}{\partial x} = \frac{JW_m C}{\dot{m}_f}, \quad (6)$$

where C is the salt concentration in the feed channel of the MD system.

The water vapor transfer through the nanochannel network in the MD membrane can be modeled as gas transport in porous media known as the dusty gas model (DGM) which is characterized by four possible mechanisms: Knudsen diffusion, molecular diffusion, surface diffusion, and viscous flow. It is common for DCMD applications to neglect the surface diffusion and viscous flow [20]. In the Knudsen diffusion regime, the gas density is so low that a gas molecule can travel without collisions with other gas molecules (i.e., long mean free path) or the diameter of the nanochannels is so small that collisions between a gas molecule and the pore wall of the nanochannels are dominant over the collisions between gas molecules. In contrast, in the molecular-diffusion regime, molecule-molecule collisions is dominant over molecule-wall collisions and the gas molecules of different species in a mixture move relative to each other under the influence of concentration gradients.

The mean free path of the flow of water molecules under typical DCMD operating conditions is comparable to the typical pore size of MD membrane materials. Therefore, the mass transport condition is at a transition regime

[20] involving collisions both between the water molecules (molecular diffusion) and between the molecules and pore wall of the membrane (Knudsen diffusion). Therefore, the mass transport in the transitional regime can be calculated by a combination of the molecular and Knudsen diffusions. The water mass flux through a nano-porous network in the MD membrane can be modeled by combining the molecular and Knudsen diffusions in series and is given by

$$J = \frac{\varepsilon_m \rho_T D_{wv-a} M_w}{\tau_m (1 - \alpha) \delta_m R T_m} \ln \left\{ \frac{D_{Kn} [\rho_T - (1 - \alpha) \rho_{v,p}] + \left[\frac{\varepsilon_m}{\tau_m} \right] \rho_T D_{wv-a}}{D_{Kn} [\rho_T - (1 - \alpha) \rho_{v,f}] + \left[\frac{\varepsilon_m}{\tau_m} \right] \rho_T D_{wv-a}} \right\}, \quad (7)$$

$$D_{Kn} = \frac{4\varepsilon_m d_p}{3\tau_m} \sqrt{\frac{RT_m}{2\pi M_w}}, \quad (8)$$

$$p_T D_{wv-a} = 1.895 \times 10^{-5} T_m^{2.072}, \quad (9)$$

$$\alpha = \frac{M_w}{M_a}, \quad (10)$$

where ε_m , τ_m , δ_m and d_p are porosity, tortuosity, thickness, and pore diameter of the membrane, respectively and their values are listed in Table 1. D_{Kn} is the diffusivity for Knudsen diffusion. $p_T D_{wv-a}$ is a product of the total pressure (p_T) and water-vapor diffusivity (D_{wv-a}) in air and has the unit of [Pa m² s⁻¹]. T_m is the membrane temperature in Kelvin and determined by the average of the local feed and permeate temperatures ($T_{m,f}$, $T_{m,p}$) on the membrane surfaces. M_w and M_a are the molecular weights of water and air, respectively.

In Eq. (7), the vapor pressures ($p_{v,f}$, $p_{v,p}$) of the feed and permeate streams are evaluated at their local fluid temperatures. For non-ideal binary mixtures with the non-volatile solute (NaCl), the partial pressure can be determined by

$$p_v = a_w (1 - M) p_{sat}, \quad (11)$$

Table 1

Dimensional and thermophysical properties of membrane and baseline operating conditions and dimension of direct contact membrane distillation system

| Dimensional and thermophysical properties of membrane | | | | | |
|---|---------------------|---|-----------------|-----------|--|
| Membrane type | δ_m (m) | d_p (m) | ε_m | τ_m | k_m (W m ⁻¹ K ⁻¹) |
| QM022 | 67×10^{-6} | 3.6×10^{-7} | 0.8 | 1.79 | 0.23 |
| Baseline operating conditions and dimensions of DCMD module | | | | | |
| $T_{f,i}$ (°C) | $T_{p,i}$ (°C) | $\dot{m}_f = \dot{m}_p$ (kg s ⁻¹) | L_m (m) | W_m (m) | $C_{f,i}$ (g L ⁻¹) |
| 70 | 40 | 1 | 1 | 1 | 35 |

where the water activity in NaCl solutions, a_w , is a function of the composition and determined by [21]

$$\alpha_w = 1 - 0.5M - 10M^2, \quad (12)$$

where M is the mole fraction of NaCl solutions. The pure water saturation pressure (p_{sat}) in the unit of Pascal can be determined by the Antoine equation and is given by [22]

$$p_{sat} = \exp\left(23.1964 - \frac{3816.44}{T - 46.13}\right), \quad (13)$$

where T is the fluid temperature in the unit of Kelvin. The presence of salt in the feed water decreases the water vapor pressure in proportion to the salt concentration, as shown in Eq. (11). For sea water with a mole fraction of 0.01 ($C = 35 \text{ g L}^{-1}$), the vapor pressure is decreased by 1.6% at 60°C.

The thermal efficiency of the DCMD system can be defined by the ratio of the phase change heat transfer to the total heat transfer across the membrane which is used to measure the efficiency of the thermal energy utilization of the membrane distillation and is given by

$$\eta_T = \frac{q_{fg}}{q_{fg} + q_k}, \quad (14)$$

where,

$$q_{fg} = W_m \int_0^{L_m} q_{fg}'' dx = W_m \int_0^{L_m} J h_{fg} dx, \text{ and} \quad (15)$$

$$q_k = W_m \int_0^{L_m} q_k'' dx = W_m \int_0^{L_m} \frac{k_m}{\delta_m} (T_f - T_p) dx. \quad (16)$$

The diesel engine loses a large portion of the combustion heat through engine cooling (about 20% of the fuel energy) and exhaust gas (about 30% of the fuel energy). In this analysis, the engine coolant is considered as the heat source for the DCMD system. A flat plate heat exchanger (HX1) is used to exchange the heat between the engine coolant and the feed stream in a counter-flow arrangement. The dimensions of the flat plate heat exchanger are listed in Table 2. The technical specifications [23] of a commercial diesel generator (Cummins, model KTA38-G9) reports that 672 kW is ejected to the engine cooling system and the temperature and flow rate of the engine coolant available for the heat exchanger are 110°C and 6.8 kg/s, respectively.

The energy supply (q_{in}) from the heat source heat exchanger (HX1) required for the DCMD system can be determined from an energy balance and is given by

$$q_{in} + \dot{m}_{b,c} c_w T_{b,i} = \dot{m}_{f,i} c_w T_{f,i} - (\dot{m}_{f,i} - \dot{m}_{b,i}) c_w T_{f,o} = N_m (q_{fg} + q_k), \quad (17)$$

Table 2
Dimensions and thermophysical property of the flat-plate heat exchanger (HX1) used for diesel engine cooling system

| L_{HX} (m) | W_{HX} (m) | a_p (m) | δ_p (m) | k_p ($\text{W m}^{-1} \text{K}^{-1}$) |
|--------------|--------------|--------------------|-----------------------|---|
| 0.87 | 0.38 | 3×10^{-3} | 0.42×10^{-3} | 13.2 |

where N_m is the number of membrane modules in the DCMD system. For the one-module system, $N_m = 1$.

From an energy balance, the temperature of the mixed flow of the brine inflow and feed water entering into the heat source heat exchanger (HX1) is determined by

$$\dot{m}_{f,o} c_w T_{f,o} = \dot{m}_b c_w T_{b,i} - \dot{m}_{f,i} c_w T_{HX,f,i}. \quad (18)$$

The energy balance for the heat exchanger (HX1) is described by

$$q_{in} = \dot{m}_{f,o} c_w (T_{f,i} - T_{HX,f,i}) = \dot{m}_{eg} c_{eg} (T_{eg,i} - T_{eg,o}). \quad (19)$$

The heat transfer area of the heat source heat exchanger (HX1) is determined using ε -NTU method [19]. The heat exchanger effectiveness (ε_{HX}) is calculated by

$$\varepsilon_{HX} = \frac{C_h (T_{h,i} - T_{h,o})}{C_{\min} (T_{h,i} - T_{c,i})}, \quad (20)$$

where, the subscript h is for the hot fluid (feed stream) and the subscript c is for cold fluid (permeate stream). For a heat exchanger in a counter flow configuration, the relation for ε and NTU is given by

$$\varepsilon_{HX} = \frac{1 - \exp[-NTU(1 - C_r)]}{1 - C_r \exp[-NTU(1 - C_r)]}, \quad (21)$$

where NTU is the number of the unit. C_r is the ratio between the minimum and maximum heat capacity rates. U is the overall heat transfer coefficient. NTU and U are determined by

$$NTU = \frac{UA}{C_{\min}}, \quad (22)$$

$$\frac{1}{U} = \frac{1}{h_h} + \frac{\delta_p}{k_p} + \frac{1}{h_c}, \quad (23)$$

where C_{\min} is the minimum heat capacity. h_h and h_c are the hot-side and cold-side convective heat transfer coefficients, respectively. δ_p and k_p are the thickness and thermal conductivity of the plate walls of the heat exchanger, respectively, and their values are listed in Table 2.

The heat source heat exchanger (HX1) was assumed to be a flat plate heat exchanger [24]. The heat transfer correlations of the flat plate heat exchanger used to calculate the convective heat transfer coefficients (h_h, h_p) are given by

$$Nu = \frac{hD_h}{k_f} = \begin{cases} \dots\dots\dots 0.44 & 0.5 & \leq & \leq \\ 0.405 \text{Re}^{0.7} \text{Pr}^{0.5} & 300 \leq \text{Re} \leq 2000 & , & (24) \\ 0.84 \text{Re}^{0.6} \text{Pr}^{0.5} & 2000 \leq \text{Re} \leq 20000 \end{cases}$$

$$\text{Re} = \frac{\left(\frac{2\dot{m}}{N_{HX}}\right) D_h}{\mu A_c}, \quad (25)$$

where \dot{m}_a is the flow rate of the feed stream or engine coolant. N_{HX} is the number of the flow channels, A_c is the cross-sectional area of the flow channels, and D_h is the hydraulic diameter of the flow channel in the flat plate heat exchanger. μ is the dynamic viscosity and k_f is the thermal conductivity and Pr is Prandtl number of the fluids. Using the dimensions of the flat plate heat exchanger in Table 2, A_c and D_h are determined by

$$A_c = a_p W_{HX}, \quad (26)$$

$$D_h = \frac{4a_p W_{HX}}{2(a_p W_{HX})}, \quad (27)$$

where a_p and W_{HX} are the channel height of the heat exchanger (the gap between the plates) and the width of the plate for the flat plate heat exchanger.

3. Results and discussions

A direct contact membrane distillation (DCMD) system running on diesel waste heat was numerically analyzed using a thermal-hydraulic network model. The DCMD system receives the waste heat from a diesel engine cooling system (heat source) via a heat source heat exchanger (HX1) to the feed loop as shown in Fig. 1a. A second heat exchanger (HX2) between the permeate stream and ambient (heat sink) was used to dissipate the heat from the permeate loop to ambient. In this study, the HX2 was assumed to be efficient and capable of maintaining the inlet temperature of the permeate stream ($T_{p,i}$) at a set temperature of 40°C. A counterflow configuration between the feed stream and engine coolant flow in HX1 was used to achieve an efficient heat exchange. The thermo-physical properties of the membrane are listed in Table 1.

In the first part of this section, a DCMD system consisting of one membrane module system was analyzed to investigate the effects of the inlet temperatures and flow rates of the feed and permeate streams and the membrane length on membrane distillation performance. The results are presented in Figs. 2–10. The operating conditions used for the analysis are the baseline conditions listed in Table 1 save for the variables subject to change. In the second part, another DCMD system consisting of multiple (N_m) membrane modules connected in a parallel arrangement (Fig. 1b) was analyzed under a constraint that the multiple module DCMD system received a fixed amount of the engine waste heat transferred via HX1 ($q_m = 672$ kW). The results are presented in Fig. 11.

Figs. 2–4 show the effects of the membrane module length (L_m) on the feed and permeate temperature, mass flux, water production rate, and thermal efficiency of the DCMD system. As shown in Fig. 2, as the membrane module length (the convective heat transfer area) increased, the outlet temperature of the feed stream decreased, but the outlet temperature of the permeate stream increased. Note that the x -direction is aligned with the feed flow direction but opposite the permeate flow direction (i.e., counterflow configuration). Fig. 2 also shows the variations in the vapor pressure difference (Δp) between the feed and

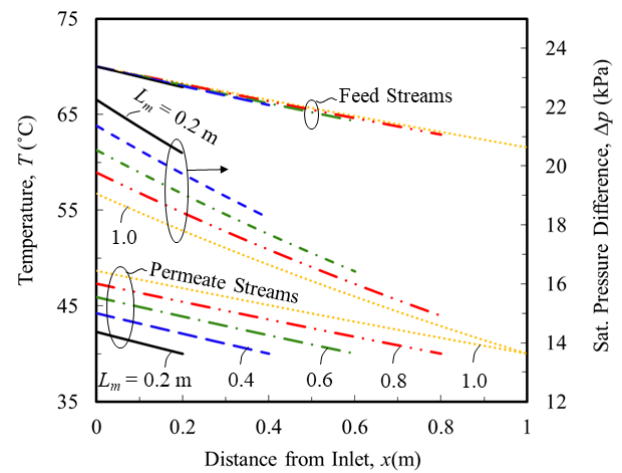


Fig. 2. Variations of feed and permeate fluid temperatures in a single-module DCMD system and the vapor pressure difference across the membrane with different membrane length under the baseline conditions.

permeate streams which rapidly decreased because of the steep change in the saturation pressure of water, especially in the feed stream at higher temperatures, according to the Antoine correlation in Eq. (13). In turn, the vapor pressure difference was much higher for shorter modules where a larger temperature difference was maintained between the feed and permeate streams.

Fig. 3(a) shows that the water mass flux (J) through the membrane was higher for shorter membrane modules and decreased according to the behavior of the vapor pressure difference in Fig. 2. The variation of the conduction and phase change heat fluxes along the membrane are shown in Fig. 3(b). The conduction heat flux [$q''_k = k_m(T_{m,f} - T_{m,p})$] remained constant due to a relatively constant temperature difference between the feed and permeate streams, while the phase change heat flux ($q''_{fg} = Jh_{fg}$) rapidly decreased like the mass flux does. The heat transfer rates for the conduction and phase change, and thermal efficiency are shown in Fig. 4a. As discussed above, a longer membrane module consumed less heat in the phase change heat transfer, q_{fg} , while the conduction heat transfer, q_k linearly increased with the membrane length and in turn, the thermal efficiency decreased. Fig. 4b shows that longer membrane modules (larger membrane area) produced more distilled water but at lower thermal efficiencies. This is due to the vapor pressure difference (water mass production) that is reduced, which consumes less heat during the phase change (evaporation and condensation), while the conduction heat loss, which is proportional to the temperature difference across the membrane, remains similar. Such an inefficient use of the heat for the membrane distillation leads to lower thermal efficiency.

Fig. 5a shows the effect of the NaCl concentration at the inlet of the feed channel on the water mass flux and the concentration variation in the feed channel for the baseline salt concentration. The baseline salt concentration is 35 g L⁻¹ (mole fraction, $M = 0.01$) which was chosen based on the salt concentration of sea water. The NaCl concentration was varied from 0 to 210 g L⁻¹. The water vapor pressure of the salt solution decreases with the salt concentration according to Eq. (11). Therefore, the mass flux decreases with the salt

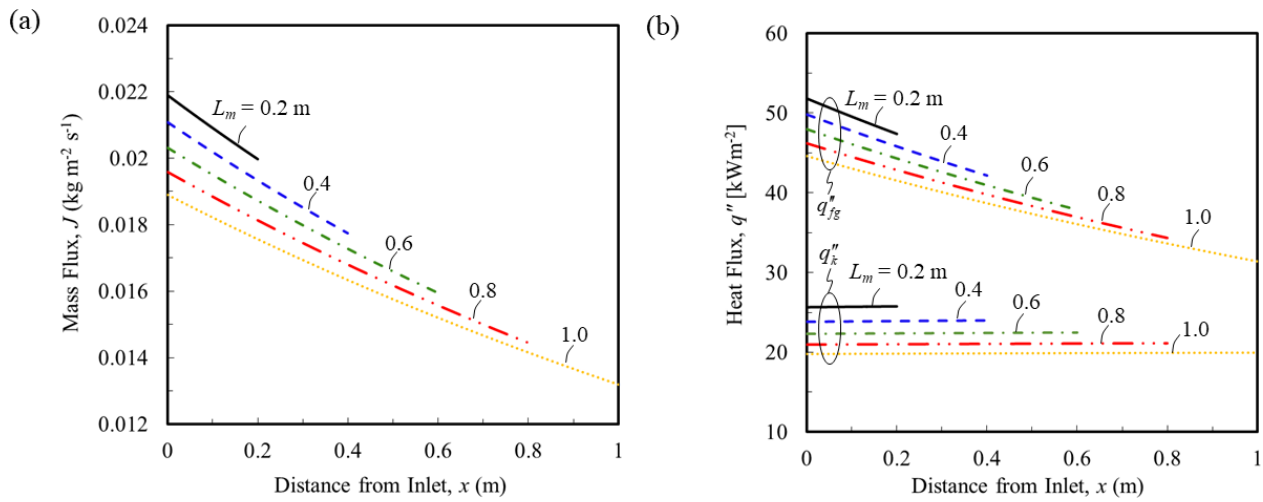


Fig. 3 (a) Variation of mass flux of water distillate production and (b) conduction and phase change heat fluxes in a single-module DCMD system with different membrane length under the baseline conditions.

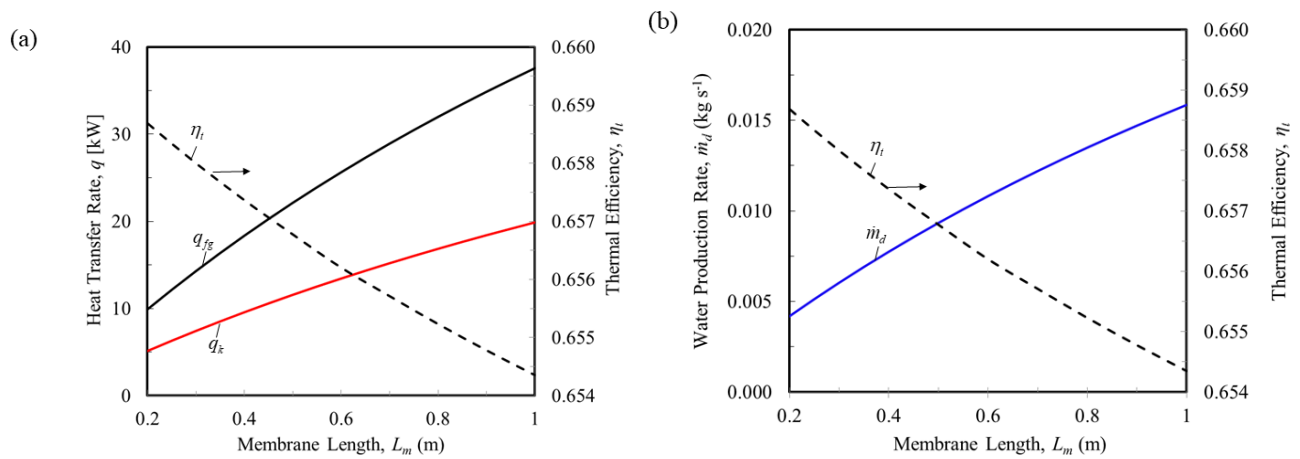


Fig. 4. Effects of membrane module length on (a) heat transfer rates and thermal efficiency and (b) total water distillate production rate in a single-module DCMD system.

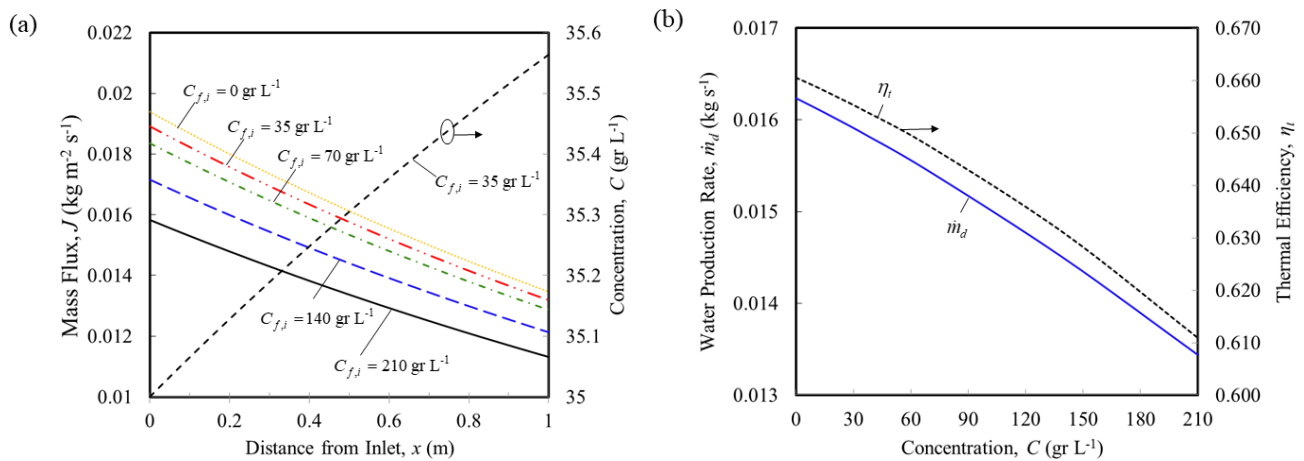


Fig. 5. (a) Variation of mass flux of water production with different inlet feed concentration and the profile of NaCl concentration along the MD channel under the baseline conditions. (b) Effect of inlet feed concentration on thermal efficiency and total water production rate in a single-module DCMD system.

concentration due to the decrease in the vapor pressure of the feed water. Since the reduction in the vapor pressure is compounded as the water is distilled along the feed stream and in turn, the solution concentration gets stronger. Fig. 5b shows that both the water production and thermal efficiency decrease similarly with respect to the salt concentration.

The effects of the feed and permeate flow rates were investigated and the results are shown in Figs. 6–8. For simplicity in the analysis, the feed and permeate flow rates were assumed to be equal. Fig. 6 shows that as the feed and permeate flow rates (sensible heat) are increased, the temperature variations of the feed and permeate waters will eventually become nearly linear by matching the energy supply and demand for the water production by evaporation and condensation. In Fig. 7, the mass flux of the water production exhibits a similar trend found in the temperature results of Fig. 6 because of the mass transfer and vapor pressure relation in a logarithmic function [Eq. (7)] and the saturation pressure and temperature relation in an exponential function [Antoine relation Eq. (13)].

The thermal efficiency and heat transfer rates for the conduction and phase change are shown in Fig. 8a. As the feed and permeate flow rates are increased, the phase change heat transfer outpaces the conduction loss and in turn, the thermal efficiency is increased. Note that the thermal efficiency increases very rapidly at the low mass flow rates which can be explained by two reasons. First, the low flow rates creates smaller temperature difference between the feed and permeate streams and in turn, smaller vapor pressure difference across the membrane as shown in Fig. 6. Secondly, the higher ratio of the mass flux for the water production to the mass flow rate [Eq. (6)] rapidly increases the concentration in the feed channel. Fig. 8b shows that the water production increases as the flow feed and permeate mass flow rates increase. Higher flow rates of the feed and permeate streams are always desirable to increase the water production and thermal efficiency. However, there would be a penalty in the increased pumping power due to the increased pressure drop in the DCMD system with the higher feed and permeate flow rates. According to the Darcy-Weisbach correlation, the pumping power increases by the square of the respective mass flow rate of the feed and permeate streams.

The effect of the inlet temperature of the feed stream on the water production is shown in Fig. 9. The permeate inlet temperature was kept at 40°C as the baseline condition, while the feed inlet temperature was varied from 45 to 70°C. Fig. 9 shows that the mass flux quickly decreased as the feed inlet temperature was decreased. This is due to the rapid decrease in the vapor pressure at relatively high temperatures.

The effects of the inlet temperatures difference (ITD, $\Delta T_i = T_{f,i} - T_{p,i}$) of the feed and permeate streams into the membrane module on the water production and thermal efficiency are illustrated in Fig. 10. The inlet temperature difference was changed by varying the inlet temperature of one fluid stream while keeping the other fluid temperature constant. In the first case, the permeate inlet temperature ($T_{p,i}$) was varied from 69 to 40°C with a fixed inlet temperature of the feed stream ($T_{f,i}$) at 70°C. In the second case, the feed inlet temperature ($T_{f,i}$) was increased from 41 to 70°C with a fixed inlet temperature of the permeate stream ($T_{p,i}$)

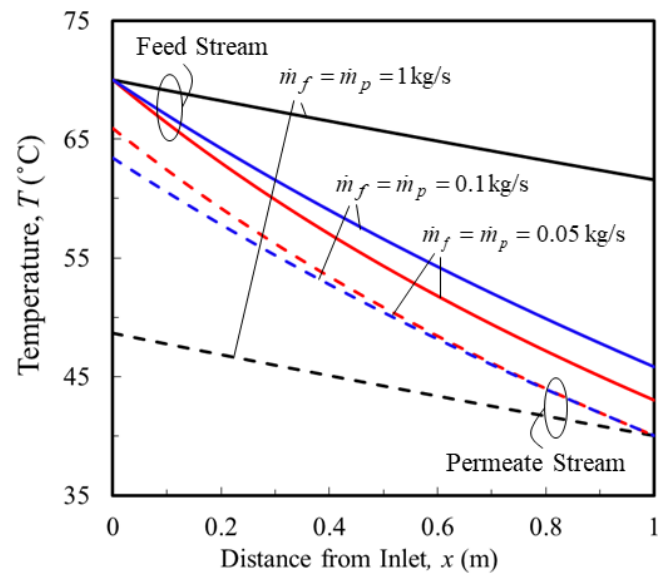


Fig. 6. Effect of feed and permeate mass flow rates on the temperature profiles of a single-module DCMD system.

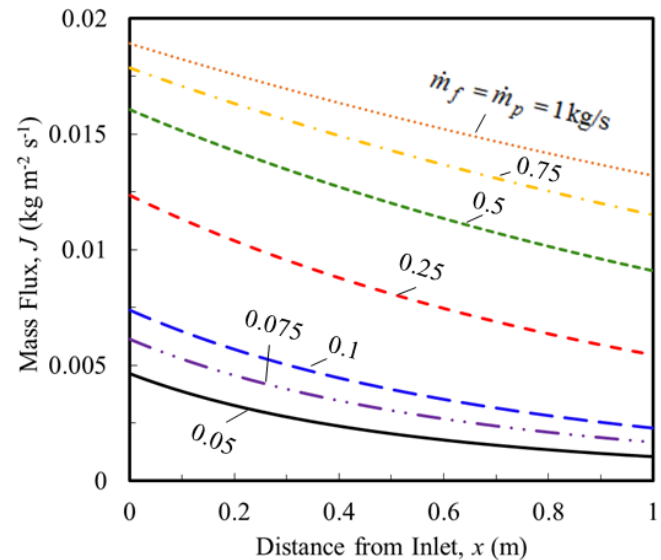


Fig. 7. Effect of feed and permeate mass flow rates on the mass flux of the water distillate production of a single-module DCMD system.

at 40°C. It is observed in Fig. 10 that the water production is increased with increasing ITD and the first case where the feed water temperature is higher, produced more efficiently water than the second case where the feed water temperature is lower. These results are attributed to the fact that conduction heat loss increases linearly with the temperature difference between fluid streams but the vapor pressure changes (phase change heat transfer) exponentially with the fluid temperature, especially at high temperatures. The optimum ITD for a maximum thermal efficiency exists around 6°C in the first case where the permeate water temperature and therefore the vapor pressure (phase change heat transfer) are decreased. In the second case, however, the thermal

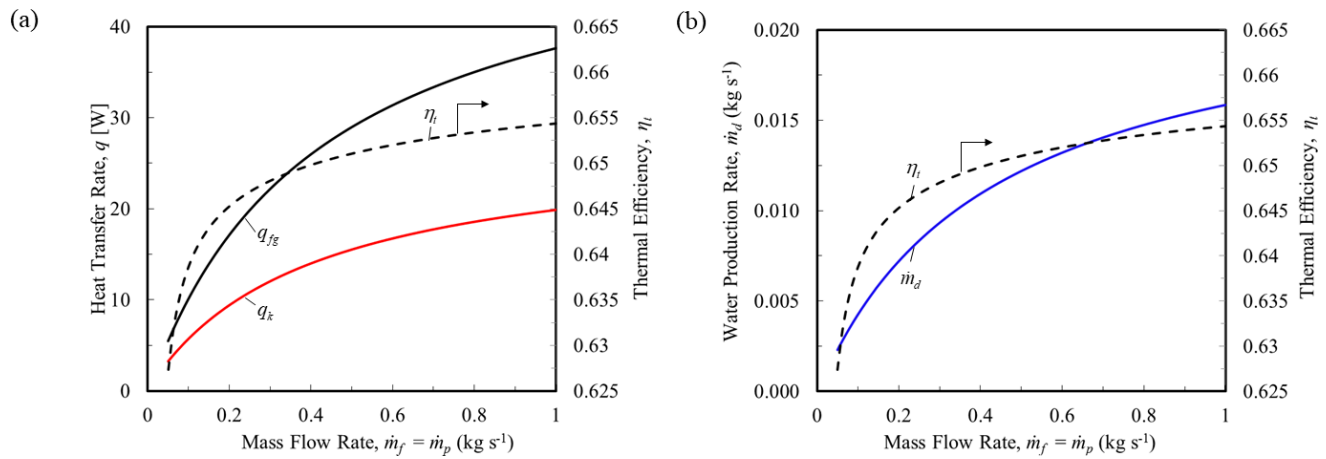


Fig. 8. Effects of feed and permeate mass flow rates on (a) the heat transfer rates and thermal efficiency and (b) total water distillate production of a single-module DCMD system.

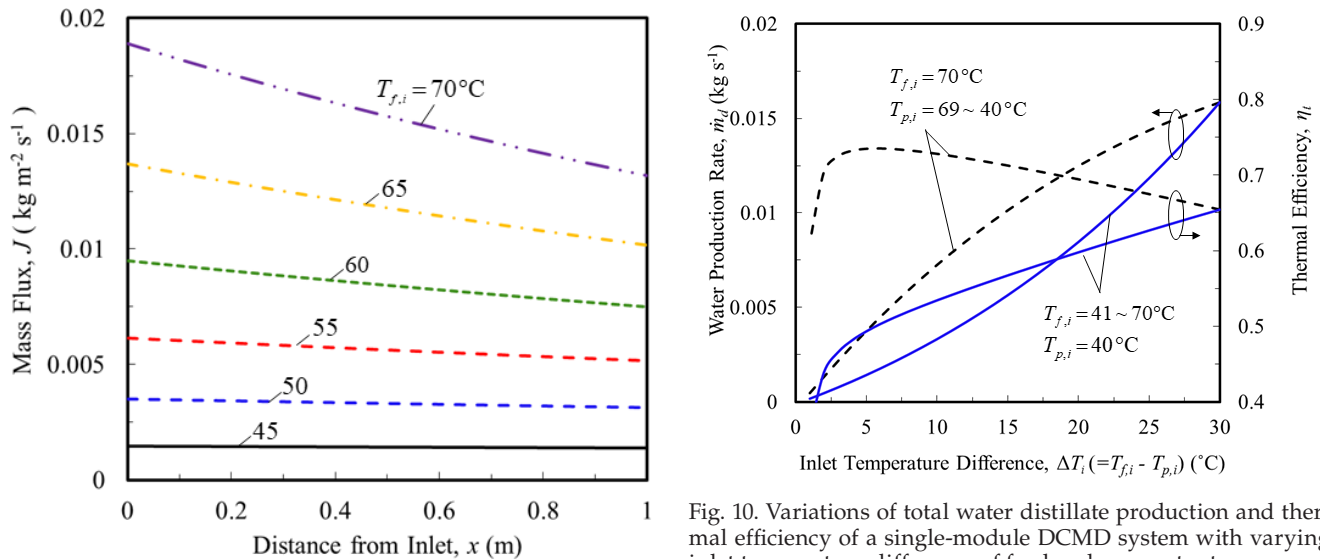


Fig. 9. Effect of feed inlet temperature on the mass flux of the water distillate production of a single-module DCMD system.

efficiency is increased continuously since the phase change heat transfer always outpaces the conduction heat loss, as the feed temperature increases. The different behaviors of the conduction and phase change heat transfers provides a useful insight for the temperature control of the fluid temperatures. To sum, it is always desirable to keep the ITD (e.g., by decreasing the permeate water temperature as in the first case and increasing the feed water temperature as in the second case) as high as possible for high thermal efficiency and more water production, only if the permeate water temperature is relatively high so that it needs to be decreased. Fig. 10 also explains how greatly the water production would be affected by the thermal performance of the heat sink heat exchanger [HX2 in Fig. 1(a)] in an attempt to keep the permeate temperature low. If the heat sink (e.g., ambient air) temperature is so high so that the cooling is not sufficient, the permeate inlet temperature rises even higher resulting in a reduction of the water production.

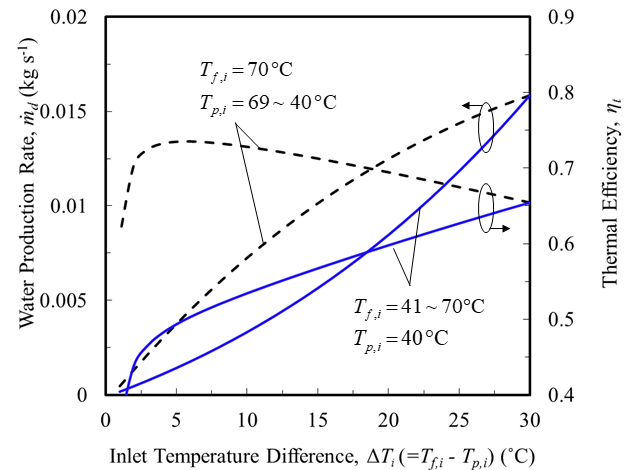


Fig. 10. Variations of total water distillate production and thermal efficiency of a single-module DCMD system with varying inlet temperature difference of feed and permeate streams.

A second DCMD system consisting of multiple membrane modules in a parallel arrangement (Fig. 1b) was analyzed under the condition that a fixed amount of energy supply (q_{in}) of 672 kW was utilized from the diesel engine coolant and the results are presented in Fig. 11. The baseline operating conditions listed in Table 1 were used in the analysis, except the membrane length. Fig. 11(a) shows the variations in the heat transfer area (A_{HX}) of HX1, the total membrane surface area (A_m), and the number of the DCMD modules (N_m) by varying the length (L_m) of the DCMD modules. A shorter module produces more water because it operates at a higher feed water temperature. As a result, the high feed water temperature enters HX1 causing a small temperature difference between the feed water and engine coolant and requiring a large heat transfer area (A_{HX}) to exchange the fixed amount of energy supply in HX1. Since a shorter DCMD module provides a smaller membrane area (A_m), a greater number (N_m) of the short membrane modules are required for water production. Although it is common to increase the heat transfer area (A_{HX}) by increasing the

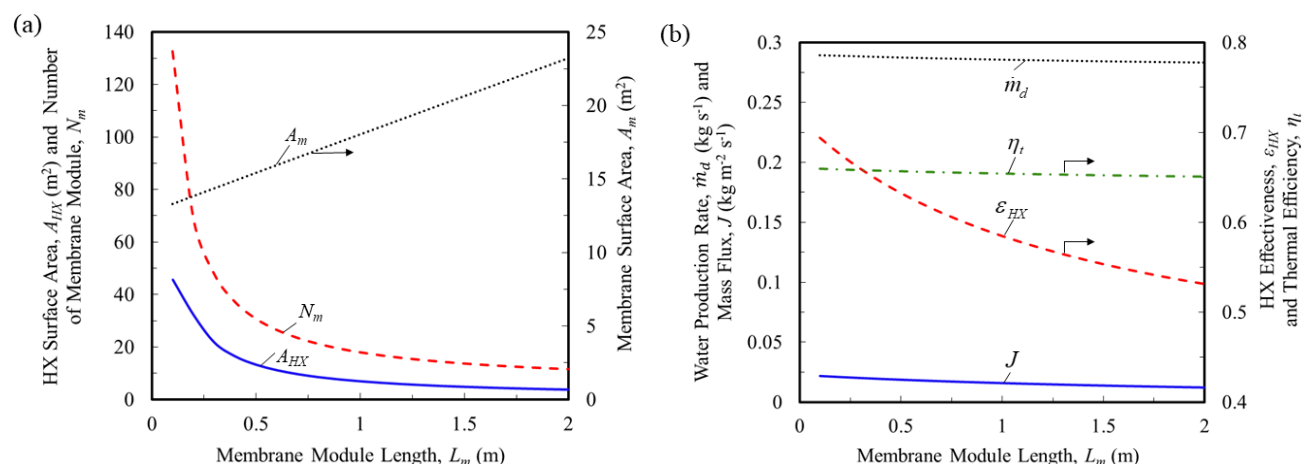


Fig. 11 (a) Variations of heat transfer area of the heat source heat exchanger (HX1), number of membrane module and total membrane area of a multiple-module DCMD system with varying membrane module length. (b) Variations of total water distillate production, mass flux, and thermal efficiency and effectiveness of the heat source heat exchanger (HX1) of a multiple-module DCMD system with varying membrane module length.

number (N_{HX}) of the flow channels in HX1, since the heat transfer coefficient is decreased due to the reduced Reynolds number, it is more desirable to choose a reasonably long membrane (e.g., $L_m = 0.5$ m) which would also lower the hardware cost associated with more modules with shorter membrane systems.

Fig. 11b shows the variations in the total water production (\dot{m}_d), mass flux (J) of the DCMD system and the heat exchanger effectiveness (ϵ_{HX}) of HX1 with respect to the length of the DCMD modules. As the membrane module gets longer, the water production (mass flux) slowly decreases, despite the increase in total membrane surface area (A_m) as shown in Fig. 11a. This is due to the heat conduction loss across the membrane which increases linearly with the membrane surface area. Thus, a longer membrane loses more heat resulting in less water production and lower thermal efficiency. The heat exchanger effectiveness of HX1 decreases for the longer DCMD module system because the inlet temperature difference between the feed (cold) and engine coolant (hot) in HX1 increases. Therefore, this is another reason to design a DCMD system with a greater number of short membrane modules to achieve higher water production, thermal efficiency, and heat exchanger effectiveness.

4. Conclusions

A thermal-hydraulic network model was developed for the Direct Contact Membrane Distillation (DCMD) systems with single and multiple flat-sheet membrane modules running on the waste heat of diesel internal combustion engine. A numerical analysis using the one-dimensional network model was performed to investigate the effects of various operating and design parameters on the water distillate production rate and thermal efficiency of the DCMD systems. The analysis suggests that a flat plate heat exchanger is a viable choice for effective heat exchange from the diesel engine to the DCMD systems. It was found from the results of the numerical analysis that the water distillate production is increased by enhancing the convective heat transfer

in the membrane channels such as increasing the flow rates and inlet temperature differences (ITD) of the feed and permeate streams. For a given ITD, higher water temperature is more desirable because of higher vapor pressure. High NaCl concentration in the feed stream lowers its vapor pressure and therefore decreases the water production. Shorter membranes produce larger water mass flux at higher thermal efficiency. For a multiple-module DCMD system, a greater number of shorter membrane modules in a parallel arrangement is more effective in the water production, as long as the heat exchanger for diesel engine waste heat recovery is large enough.

Acknowledgement

The authors extend their thanks for the financial support of the U.S. Department of Defense (DOD) and Strategic Environmental Research and Development Program (SERDP) (Contract No. W912HQ-14-C-0051) and National Science Foundation (IIA-1301726 and CAREER Award 1464504). The authors would also like to thank Dr. Vahid Vandadi at the University of Nevada, Reno for his valuable comments and initial work on the modeling. The authors alone are responsible for any omissions or other errors.

Symbols

| | | |
|------------|---|---|
| A | — | Area [m ²] |
| a_p | — | Channel height of heat exchanger [m] |
| a_w | — | Water activity [–] |
| C | — | Heat capacity $C = \dot{m} c$ [W K ⁻¹], concentration [gr L ⁻¹] |
| c | — | Specific heat capacity [J kg ⁻¹ K ⁻¹] |
| D_h | — | Hydraulic diameter [m] |
| D_{Kn} | — | Knudsen diffusion coefficient [m ² s ⁻¹] |
| D_{wv-a} | — | Diffusivity of water vapor-air mixture [m ² s ⁻¹] |
| d | — | Diameter [m] |

| | |
|-----------|--|
| h | — Heat transfer coefficient [$\text{W m}^{-2} \text{K}^{-1}$] |
| h_g | — Latent heat [J kg^{-1}] |
| J | — Mass flux [$\text{kg m}^{-2} \text{s}^{-1}$] |
| k | — Thermal conductivity [$\text{W m}^{-1} \text{K}^{-1}$] |
| L | — Length [m] |
| M | — Molecular weight [kg mol^{-1}], mole fraction [–] |
| \dot{m} | — Mass flow rate [kg s^{-1}] |
| N | — Number of flow channels of heat exchanger, number of membrane module |
| Nu | — Nusselt number |
| NTU | — Number of transfer unit |
| p | — Pressure [Pa] |
| Pr | — Prandtl number |
| q | — Heat transfer rate [W] |
| q'' | — Heat flux [kW m^{-2}] |
| R | — Gas constant [$\text{J mol}^{-1} \text{K}^{-1}$], thermal resistance [K m W^{-1}] |
| Re | — Reynolds number |
| T | — Temperature [K] or [°C] |
| U | — Overall heat transfer coefficient [$\text{W m}^{-2} \text{K}^{-1}$] |
| W | — Width [m] |
| x | — Coordinate [m] |

Greek

| | |
|---------------|---|
| α | — Ratio of water molecular weight to air molecular weight |
| δ | — Thickness [m] |
| ε | — Porosity, effectiveness |
| η | — Efficiency |
| μ | — Viscosity [N s m^{-2}] |
| τ | — Tortuosity |

Subscripts

| | |
|-------|-----------------------------------|
| a | — Air |
| amb | — Ambient |
| b | — Brine |
| c | — Conduction, cross section, cold |
| d | — Distillate |
| e | — Effective |
| eg | — Engine coolant |
| f | — Feed, fluid |
| fg | — Phase change |
| h | — Hot, hydraulic |
| HX | — Heat exchanger |
| i | — Inlet |
| k | — Conduction |
| in | — Incoming |
| m | — Membrane |
| min | — Minimum |
| o | — Outlet, outside |
| out | — Outgoing |
| p | — Permeate, pore, plate |
| r | — Ratio |
| s | — Solid, salt |
| sat | — Saturation |
| T | — Total |
| t | — Thermal |
| v | — Vapor |
| w | — Water |
| wv | — Water vapor |

References

- [1] K.W. Lawson, D.R. Lloyd, Membrane distillation, *J. Membr. Sci.*, 124 (1997) 1–25.
- [2] D. Winter, J. Koschikowski, D. Düver, P. Hertel, U. Beuscher, Evaluation of MD process performance: effect of backing structures and membrane properties under different operating conditions, *Desalination*, 323 (2013) 120–133.
- [3] M. Findley, V. Tanna, Y. Rao, C. Yeh, Mass and heat transfer relations in evaporation through porous membranes, *AIChE J.*, 15 (1969) 483–489.
- [4] A. Alkudhiri, N. Darwish, N. Hilal, Membrane distillation: A comprehensive review, *Desalination*, 287 (2012) 2–18.
- [5] J. Koo, S. Lee, J.-S. Choi, T.-M. Hwang, Theoretical analysis of different membrane distillation modules, *Desal. Water Treat.*, 54 (2015) 862–870.
- [6] M.M.A. Shirazi, A. Kargari, D. Bastani, L. Fatehi, Production of drinking water from seawater using membrane distillation (MD) alternative: direct contact MD and sweeping gas MD approaches, *Desal. Water Treat.*, 52 (2014) 2372–2381.
- [7] J. Koo, J. Han, J. Sohn, S. Lee, T.-M. Hwang, Experimental comparison of direct contact membrane distillation (DCMD) with vacuum membrane distillation (VMD), *Desal. Water Treat.*, 51 (2013) 6299–6309.
- [8] Y. Shin, J. Choi, T. Lee, J. Sohn, S. Lee, Optimization of dewetting conditions for hollow fiber membranes in vacuum membrane distillation, *Desal. Water Treat.*, 57 (2016) 7582–7592.
- [9] K. Zhani, K. Zarzoum, H. Ben Bacha, J. Koschikowski, D. Pfeifle, Autonomous solar powered membrane distillation systems: state of the art, *Desal. Water Treat.*, 57 (2016) 23038–23051.
- [10] R.B. Saffarini, E.K. Summers, H.A. Ararat, Economic evaluation of stand-alone solar powered membrane distillation systems, *Desalination*, 299 (2012) 55–62.
- [11] F. Suárez, S.W. Tyler, A.E. Childress, A theoretical study of a direct contact membrane distillation system coupled to a salt-gradient solar pond for terminal lakes reclamation, *Water Res.*, 44 (2010) 4601–4615.
- [12] R. Sarbatly, C.-K. Chiam, Evaluation of geothermal energy in desalination by vacuum membrane distillation, *Appl. Energy*, 112 (2013) 737–746.
- [13] J.C. Vega-Beltrán, L. García-Rodríguez, I. Martín-Mateos, J. Blanco-Gálvez, Solar membrane distillation: theoretical assessment of multi-stage concept, *Desal. Water Treat.*, 18 (2010) 133–138.
- [14] J.B. Rodríguez, V.M. Gabet, G.M. Monroy, A.B. Puerta, I.F. Barrio, Distilled and drinkable water quality produced by solar membrane distillation technology, *Desal. Water Treat.*, 51 (2013) 1265–1271.
- [15] Noblis, Strategic Environmental and Development Program (SERDP): Sustainable Forward Operating Bases, DOD, ed., 2010.
- [16] J. Phattaranawik, R. Jiraratananon, A. Fane, C. Halim, Mass flux enhancement using spacer filled channels in direct contact membrane distillation, *J. Membr. Sci.*, 187 (2001) 193–201.
- [17] L. Martínez-Díez, M.I. Vázquez-González, Temperature and concentration polarization in membrane distillation of aqueous salt solutions, *J. Membr. Sci.*, 156 (1999) 265–273.
- [18] R. Schofield, A. Fane, C. Fell, R. Macoun, Factors affecting flux in membrane distillation, *Desalination*, 77 (1990) 279–294.
- [19] T.L. Bergman, F.P. Incropera, D.P. DeWitt, A.S. Lavine, Fundamentals of heat and mass transfer, John Wiley & Sons, 2011.
- [20] J. Phattaranawik, R. Jiraratananon, A. Fane, Effect of pore size distribution and air flux on mass transport in direct contact membrane distillation, *J. Membr. Sci.*, 215 (2003) 75–85.
- [21] T.-C. Chen, C.-D. Ho, H.-M. Yeh, Theoretical modeling and experimental analysis of direct contact membrane distillation, *J. Membr. Sci.*, 330 (2009) 279–287.
- [22] M.A.E.-R. Abu-Zeid, Y. Zhang, H. Dong, L. Zhang, H.-L. Chen, L. Hou, A comprehensive review of vacuum membrane distillation technique, *Desalination*, 356 (2015) 1–14.
- [23] Cummins, https://www.americasgenerators.com/uploads/docs/Cummins_Generator_Engine_KTA38-G9.pdf.
- [24] B. Sundén, R.M. Manglik, Plate heat exchangers: design, applications and performance, Wit Press, 2007.